

Diffraction dissociation, an important background to photon-photon collisions via heavy ion beams at LHC

R. Engel

*Institut für Theoretische Physik,
Universität Leipzig, D-04109 Leipzig, Germany
and Universität Siegen,
Fachbereich Physik, D-57068 Siegen, Germany*

M.A. Braun*, C. Pajares and J. Ranft

*Departamento de Física de Partículas,
Universidad de Santiago de Compostela,
E-15706 Santiago de Compostela, Spain*

June 18, 1996

Abstract

The cross sections for the production of hadrons in quasi-real photon-photon collisions in proton-proton and heavy ion interactions are compared with the corresponding cross sections for central diffraction and for photon-pomeron collisions. The signatures, heavy ions or protons with only slightly changed momenta together with two large rapidity gaps and a cluster of produced hadrons in the central region, are nearly identical in all three processes. Therefore, it will be rather difficult to distinguish the reactions experimentally. It is found, that central diffraction is the dominant process in collisions of protons, light and medium-heavy ions. The photon-pomeron and photon-photon processes have quite similar cross sections in collisions of heavy ions like lead.

*Visiting professor IBERDROLA. Permanent address: Department of High Energy Physics, University of St. Petersburg, 198904 Russia

1 Introduction

Double-photon exchange as well as double-pomeron exchange and photon-pomeron reactions are characterized by large rapidity gaps separating the remnants of the colliding hadrons or heavy ions from the particles produced in the central rapidity region. This feature is likely to give a considerable reduction of the background to the studied reaction.

Photon-photon collisions in proton-proton or heavy ion reactions have been discussed repeatedly [1, 2, 3, 4, 5] as a very attractive reaction channel. Processes studied include Higgs production [6, 7, 8, 9, 10] and production of SUSY particles [9, 11]. Also the ALICE Collaboration discusses this option for the heavy ion experiment at the Large Hadron Collider (LHC) of CERN [12].

Central diffraction (CD) and especially hard central diffraction is recognized as an interesting new reaction channel at future hadron and heavy ion colliders at least since the first model for diffractive hard scattering due to Ingelman and Schlein [13] and the pioneering experiment of the UA8 Collaboration [14, 15]. For example, Higgs production in this channel was discussed in Refs. [16, 17, 18, 19] and the production of heavy flavors was studied in Refs. [20, 21, 22, 23]. The resonance and glueball production in photon-photon collisions and in central diffraction was compared in Refs. [24, 25].

Here we will discuss both processes and in addition photon-pomeron collisions for the same reactions in the framework of the two-component Dual Parton Model (DPM) [26, 27, 28] and in particular in the version as implemented in the DPM event generator PHOJET [29, 30]. We restrict the paper to the calculation of cross sections for hadron production in the three processes, in a later step we might extend the calculation to cross sections for heavy flavor or new particle production.

Hadronic photon-photon collisions within this framework were already studied and compared to data in a recent paper by Engel and Ranft [30] mainly for photon-photon collisions at electron-positron colliders. Here we report about the extension of the PHOJET model to photon fluxes as expected at proton-proton and heavy ion colliders.

Hard diffraction within the two-component DPM was first studied and compared to UA8 data and data from HERA by Engel, Ranft, and Roesler [31]. In the present paper we will calculate central diffraction cross sections as well as photon-pomeron cross sections for proton-proton and heavy ion collisions. Using these cross sections we compare basic features of the three reactions, double-pomeron, double-photon and photon-pomeron interactions at proton-proton and heavy ion colliders, which have very similar experimental signatures. A second more detailed study of particle production in double-pomeron and double-photon scattering, also using the PHOJET event generator will be published soon [32].

In Section 2 we describe the models used. Section 3 gives a detailed comparison of the cross sections and hadron distributions expected in the three channels.

A summary is given in Section 4 and in the Appendix we collect all the details about photon flux calculations in heavy ion reactions as used in this paper.

2 The Models

2.1 The event generator PHOJET

The realization of the DPM with a soft and a hard component in PHOJET is similar to the event generator DTUJET-93 [27, 33] simulating pp and $p\bar{p}$ collisions up to very high energies. PHOJET is applicable to collisions of stable hadrons as well as of photons. Here we give only a short summary on the physics of PHOJET, for more detailed descriptions we refer to [29, 30, 32, 34, 35].

The interactions of hadrons and the hadronic fluctuations of the photon are described within the Dual Parton Model in terms of reggeon and pomeron exchanges. The physical photon state is treated as a superposition of a “bare photon” and virtual hadronic states having the same quantum numbers as the photon. For soft processes, photon-hadron duality is used. The energy-dependences of the reggeon and pomeron amplitudes are assumed to be the same for all hadronic processes. Therefore, data on hadron-hadron and photon-hadron cross sections can be used to determine the parameters necessary to describe soft photon-photon interactions. Inelastic interactions are subdivided into processes involving only *soft* processes and all the other processes with at least one large momentum transfer (*hard* processes) by applying a transverse momentum cutoff $p_{\perp}^{\text{cutoff}}$ to the partons. On Born-graph level, for example, the photon-photon cross section is built up by: **(i)** soft reggeon and pomeron exchange, **(ii)** hard double-resolved photon-photon interaction, **(iii)** hard single-resolved interactions, and **(iv)** hard direct interactions. The Parton Model calculations of the hard processes have been done using the leading order GRV parton distribution functions for the proton [36] and the photon [37].

The amplitudes corresponding to the one-pomeron exchange between the hadronic fluctuations of the photon are unitarized applying a two-channel eikonal formalism similar to [27]. In impact parameter representation, the eikonalized scattering amplitude for resolved photon interactions has the structure

$$a_{\text{res}}(s, B) = \frac{i}{2} \left(\frac{e^2}{f_{q\bar{q}}^2} \right)^2 \left(1 - e^{-\chi(s, B)} \right) \quad (1)$$

with the eikonal function

$$\chi(s, B) = \chi_S(s, B) + \chi_H(s, B) + \chi_D(s, B) + \chi_C(s, B). \quad (2)$$

Here, $\chi_i(s, B)$ denote the contributions from the different Born graphs: (S) soft part of the pomeron and reggeon, (H) hard part of the pomeron (D) triple- and

loop-pomeron graphs, (C) double-pomeron graphs. In PHOJET the last two terms are included in the unitarization whereas in DTUJET they are taken in lowest order. The amplitude for hadron-hadron interactions has the same structure as (1) but without the couplings $e/f_{q\bar{q}}$ of the photon to the hadronic fluctuations.

The probabilities to find a photon in one of the generic hadronic states, the reggeon and pomeron coupling constants, and the effective reggeon and pomeron intercepts cannot be determined by basic principles. These quantities are treated as free parameters and determined by cross section fits [29]. In Refs. [29, 30] the model predictions for the proton-proton, photon-proton, and photon-photon cross sections are shown and compared to data.

The probabilities for the different final state configurations are calculated from the discontinuity of the scattering amplitude (optical theorem) which can be expressed as a sum of graphs with k_c soft pomeron cuts, l_c hard pomeron cuts, m_c triple- or loop-pomeron cuts, and n_c double-pomeron cuts by applying the Abramovski-Gribov-Kancheli cutting rules [38, 39]. In impact parameter space one gets for the inelastic cross sections

$$\sigma(k_c, l_c, m_c, n_c, s, B) = \frac{(2\chi_S)^{k_c}}{k_c!} \frac{(2\chi_H)^{l_c}}{l_c!} \frac{(2\chi_D)^{m_c}}{m_c!} \frac{(2\chi_C)^{n_c}}{n_c!} \exp[-2\chi(s, B)]. \quad (3)$$

Since the triple-, loop-, and double-pomeron graphs are objects involving several pomerons, a further resummation is done [27, 35] to allow the probability interpretation of Eq. (3).

For pomeron cuts involving a hard scattering, the complete parton kinematics and flavors/colors are sampled according to the Parton Model using a method similar to [40], extended to direct processes. For pomeron cuts without hard large momentum transfer, the partonic interpretation of the Dual Parton Model is used: photons or mesons are split into a quark-antiquark pair whereas baryons are approximated by a quark-diquark pair. The longitudinal momentum fractions of the soft partons are given by Regge asymptotics [41, 42]. The transverse momenta of the soft partons are sampled from an exponential distribution in order to get a smooth transition between the transverse momentum distributions of the soft constituents and the hard scattered partons.

In diffraction dissociation or double-pomeron scattering, the parton configurations are generated using the ideas of the two-component DPM applied to pomeron-hadron, photon-pomeron and pomeron-pomeron scattering processes (see [31] and references therein). For the parton densities in the pomeron we use the CKMT parametrization [43].

Finally, the fragmentation of the sampled partonic final states is done by forming color neutral strings between the partons according to the color flow. In the limit of large number of colors in QCD, this leads to the two-chain configuration characterizing a cut pomeron and a one-chain system for a cut reggeon. The chains are fragmented using the Lund fragmentation code JETSET 7.3 [44].

2.2 Diffraction dissociation in the two-component Dual Parton Model

2.2.1 Single diffraction dissociation

In the model, low- and high-mass diffraction dissociation is distinguished. Low-mass diffraction dissociation is described by assuming the scattering of a superposition of resonances with the quantum numbers of the dissociating particle [45]. For simplicity, only one generic resonance is considered in the model. In this case, the cross section of diffractive processes with low-mass final states ($M_D^2 < 2 \text{ GeV}^2/c^4$) can be calculated using a two-channel eikonal formalism [46, 27, 29]. In the limit of large diffractive masses $s \gg M_D^2 \gg s_0$ and $M_D^2 \gg t$ with $s_0 \approx 1 \text{ GeV}^2$, the data can be understood in terms of the triple-pomeron graph [46, 47]. Here, M_D denotes the diffractively produced mass and t is the squared four-momentum transfer. In Fig. 1, the triple-pomeron graph and the corresponding diffractive cut for diffractive dissociation of particle A and quasi-elastic deflection of particle B is shown. Assuming multiperipheral kinematics of the pomeron cut final states, the rapidity gap is approximately given by $\eta_{\text{gap}} \approx \ln(s/M_D^2)$. It is convenient to characterize the final state using the Feynman x_F of the elastically scattered particle B

$$x_B = - \left(1 - \frac{M_D^2}{s} \right) \quad (4)$$

which leads to

$$M_D^2 \approx (1 - |x_B|)s \quad \text{and} \quad \eta_{\text{gap}} \approx \ln \left(\frac{1}{1 - |x_B|} \right) \quad (5)$$

In Born-graph approximation neglecting rescattering effects, the double-differential cross section for high-mass diffraction dissociation reads

$$\begin{aligned} \frac{d^2 \sigma_{\text{TP}}}{dt dM_D^2} &= \frac{1}{16\pi} (g_{AP}^0)^2 g_{PP}^0 g_{BP}^0 \left(\frac{s}{s_0} \right)^{2\Delta_P} \left(\frac{s_0}{M_D^2} \right)^{\alpha_P(0)} \\ &\times \exp \left\{ \left(b_{AP} + b_{PP} + 2\alpha'_P(0) \ln \left(\frac{s}{M_D^2} \right) \right) t \right\}. \end{aligned} \quad (6)$$

with $\Delta_P = \alpha_P(0) - 1$, $\alpha_P(0)$ being the pomeron intercept. The coupling constants are parametrized by

$$g_{iP}(t) = g_{iP}^0 \exp \left(\frac{1}{2} b_{iP} t \right) \quad i = A, B \quad (7)$$

$$g_{PPP}(t_1, t_2, t_3) = g_{PPP}^0 \exp \left(\frac{1}{2} b_{PPP} (t_1 + t_2 + t_3) \right). \quad (8)$$

In the following we will restrict the diffractively produced mass according to an experimentally motivated cut on the Feynman x_F of the elastically scattered particle [20]

$$|x_B| > c, \quad M_{D,\min}^2 \leq M_D^2 \leq (1-c)s, \quad (9)$$

with $c = 0.9 \dots 0.97$. The integration over t and M_D^2 can be performed analytically [48]

$$\begin{aligned} \sigma_{\text{TP}} &= \frac{1}{16\pi} \left(\frac{s}{s_0}\right)^{\Delta_P} \frac{(g_{AP}^0)^2 g_{PPP}^0 g_{BP}^0}{2\alpha'_P(0)} \\ &\times \exp \left\{ -\Delta_P \frac{b_{AP} + b_{PPP}}{2\alpha'_P(0)} \right\} \\ &\times \left[Ei \left(\Delta_P \left(\frac{b_{AP} + b_{PPP}}{2\alpha'_P(0)} + \ln \frac{s}{M_{D,\min}^2} \right) \right) \right. \\ &\quad \left. - Ei \left(\Delta_P \left(\frac{b_{AP} + b_{PPP}}{2\alpha'_P(0)} + \ln \frac{1}{1-c} \right) \right) \right], \quad (10) \end{aligned}$$

where Ei denotes the second exponential integral function.

Elastic and inelastic rescattering effects decrease the cross section as given by Eq. (6) considerably [49, 50]. This suppression is estimated using the eikonal model as described in the previous section. In impact parameter representation, the experimentally observable cross section of diffraction dissociation follows from (see Eq. (3))

$$\sigma^d(s, B) = \sigma(k_c = 0, l_c = 0, m_c = 1, n_c = 0; s, B). \quad (11)$$

The free parameters of the model (coupling constants, pomeron intercept, slope parameters) are determined by a global fit to data on total, elastic and diffractive cross sections as well as data on elastic slope of pp , $p\bar{p}$ and γp interactions [29]. Assuming that soft hadronic interactions in hadron-hadron, photon-hadron, and photon-photon interactions can be described by the exchange of one universal object, the pomeron, all these data can be combined to increase the predictive power of the model.

Fig. 1 suggests the interpretation of photon diffraction in terms of photon-pomeron scattering. However, since the pomeron is only a theoretically introduced object to describe the some features of hadronic high-energy scattering, it is not possible to consider photon-pomeron scattering without the corresponding hadron where the pomeron couples to.

Finally, it should be mentioned that the model results can be compared with the new measurements on the cross section of photon single diffraction dissociation at HERA. This is important since the cross section on photon diffraction dissociation enters directly the predictions on the photon-pomeron cross sections. For $\sqrt{s_{\gamma p}} = 200$ GeV, the model predicts a cross section of $19\mu\text{b}$ to be compared

with $23 \pm 11 \mu\text{b}$ [51]. Furthermore, in Ref. [51], some model results are shown together with data on photon diffraction obtained by the H1 Collaboration, finding reasonable agreement.

2.2.2 Central diffraction

A direct consequence of the interpretation of diffraction as pomeron-particle scattering is the prediction of the existence of pomeron-pomeron scattering (double-pomeron scattering). Double-pomeron cross sections in hadron-hadron collisions were first calculated on the basis of single diffractive measurements and Regge theory by Chew and Chew [52] and by Kaidalov and Ter-Martirosyan [53]. Using different models, these calculations have been continuously extended to partial cross section estimations (see for example Refs. [54, 55] and references therein).

The calculation of double-pomeron cross sections is subject to considerable uncertainty. There are several reasons for this:

- (i) The cross section is proportional to the square of the triple-pomeron coupling constant g_{PPP} , which is not very well known.
- (ii) The double-pomeron cross section differs considerably, if this term is included into an unitarization procedure for all hadronic cross sections or not. For example, it was discussed recently [56], that the effects of shadowing decrease the double-pomeron cross sections at LHC energies by a factor of 5. The cross section estimates as given for example in [53, 20] do not include any unitarization whereas in our approach the double-pomeron cross sections are included in the unitarization.
- (iii) The energy dependence of the double-pomeron cross section might differ considerably when using either a critical or a supercritical pomeron intercept $\alpha_P(0)$. In [53, 20] a critical pomeron intercept $\alpha_P(0) = 1$ was used. Here we use, consistent with high-energy cross section measurements, a supercritical intercept $\alpha_P(0) > 1$.
- (iv) On a more practical level these cross sections depend on the cuts applied to the centrally produced cluster of particles and on the rapidity gaps demanded by the experimental triggers.
- (v) In CD, one or both of the incoming hadrons can be excited to a resonance N^* . In the following, for the comparison with the two-photon cross sections, we exclude from the calculation all cross section contributions involving resonances. Including these contributions would about double the cross sections given below. These contributions would also change the rapidity gap demanded in experimental trigger conditions.

In the approximation of multiperipheral kinematics, the mass M_{cd} of the centrally produced diffractive system is $M_{cd}^2 = (s_1 s_2)/s$ (see Fig. 2). The rapidity gaps between the central system and the elastically scattered particles can be

approximated by

$$\eta_{\text{gap1}} \approx \ln\left(\frac{s}{s_2}\right) \quad \eta_{\text{gap2}} \approx \ln\left(\frac{s}{s_1}\right) . \quad (12)$$

Denoting the Feynman x_F of the elastically scattered particles A and B by x_A and x_B one gets [20]

$$x_A = 1 - \frac{s_2}{s} \quad x_B = -\left(1 - \frac{s_1}{s}\right) \quad (13)$$

and

$$\begin{aligned} M_{cd}^2 &\approx (1 - |x_A|)(1 - |x_B|)s \\ \eta_{\text{gap1}} &\approx \ln\left(\frac{1}{1 - |x_A|}\right) \quad \eta_{\text{gap2}} \approx \ln\left(\frac{1}{1 - |x_B|}\right) . \end{aligned} \quad (14)$$

Within the framework of Gribov's Reggeon calculus, the amplitude of the double-pomeron graph can be calculated (for more details see [53, 32]). From this one gets the cross section as function of t_A , t_B , s_1 , and s_2 (t_A and t_B denote the squared momentum transfer of particle A and B). After integration over t_A and t_B the differential cross section reads

$$\begin{aligned} \frac{d\sigma_{\text{DP}}}{ds_1 dM_{cd}^2} &= \frac{1}{256\pi^2} \sigma_{\text{PPP}}(M_{cd}^2) \left(\frac{s}{M_{cd}^2}\right)^{2\Delta_P} \frac{1}{M_{cd}^2} \frac{1}{s_1} \\ &\times \frac{(g_{AP}^0)^2}{b_{AP} + b_{PPP} + 2\alpha'_P(0) \ln\left(\frac{s_1}{M_{cd}^2}\right)} \\ &\times \frac{(g_{BP}^0)^2}{b_{BP} + b_{PPP} + 2\alpha'_P(0) \ln\left(\frac{s}{s_1}\right)} \end{aligned} \quad (15)$$

with

$$\sigma_{\text{PPP}}(M_{cd}^2) = (g_{\text{PPP}}^0)^2 \left(\frac{M_{cd}^2}{s_0}\right)^{\Delta_P} . \quad (16)$$

Applying the previously discussed cut on the Feynman x_F of the elastically scattered hadrons

$$\begin{aligned} x_A &\geq c, & |x_B| &\geq c, \\ M_{cd,\text{min}}^2 &\leq M_{cd}^2 \leq (1 - c)^2 s \end{aligned} \quad (17)$$

the integration over s_1 can be performed

$$\frac{M_{cd}^2}{1 - c} \leq s_1 \leq (1 - c)s \quad (18)$$

$$\begin{aligned}
M_{cd}^2 \frac{d\sigma_{\text{DP}}}{dM_{cd}^2} &= \frac{1}{256\pi^2} \sigma_{\text{PP}}(M_{cd}^2) (g_{\text{AP}}^0 g_{\text{BP}}^0)^2 \\
&\times \frac{1}{\alpha'_{\text{P}}(0)} \left(\frac{s}{M_{cd}^2} \right)^{2\Delta_{\text{P}}} \\
&\times \ln \left(\frac{b_{\text{AP}} + b_{\text{PPP}} + 2\alpha'_{\text{P}}(0) \ln((1-c)s/M_{cd}^2)}{b_{\text{BP}} + b_{\text{PPP}} + 2\alpha'_{\text{P}}(0) \ln(1/(1-c))} \right) \\
&\times (b_{\text{AP}} + b_{\text{BP}} + 2b_{\text{PPP}} + 2\alpha'_{\text{P}}(0) \ln(s/M_{cd}^2))^{-1} .
\end{aligned} \tag{19}$$

In order to calculate the cross section for CD, the Born graph cross section (19) for double-pomeron scattering is included in the eikonalization. In impact parameter representation, the CD cross section reads (see Eq. (3))

$$\sigma^{cd}(s, B) = \sigma(k_c = 0, l_c = 0, m_c = 0, n_c = 1; s, B) . \tag{20}$$

In Fig. 3 we compare as function of the energy the CD cross sections in proton-proton collisions, which we obtain from PHOJET with the cross section obtained by Streng [20]. For both calculations the same three kinematical cuts are used: $M_{cd} > 2\text{GeV}/c^2$ and $c = 0.90, 0.95$ and 0.97 . In PHOJET we use a supercritical pomeron with $\Delta_{\text{P}} = 0.08$ whereas Streng [20] uses a critical Pomeron with $\Delta_{\text{P}} = 0$. Note that the double-pomeron cross section grows in Born approximation with s like $\sim s^{2\Delta_{\text{P}}}$. This rapid increase is damped in PHOJET by the unitarization procedure. At high energies, contributions from multiple interactions become important. The demanded rapidity gaps are filled with hadrons due to inelastic rescattering and the cross section for CD gets strongly reduced. In contrast, Streng calculates only the Born term cross section. Figure 3 illustrates the differences obtained using different methods. We stress, both methods use the measured single diffractive cross sections to extract the triple-pomeron coupling.

Finally, it should be mentioned that in a very recent work [57] pomeron-pomeron cross sections have been studied in the perturbative BFKL-Bartels approach (see [57] and references therein). The predictions on cross sections found in this work are of the same order as the ones obtained here.

2.3 Diffractive cross sections in collisions involving nuclei

2.3.1 Central diffraction cross sections in heavy ion collisions

There are certain difficulties in resolving the CD cross section as a function of its central mass M_{cd} in hadron-nucleus and nucleus-nucleus collisions. In fact, consider the simplest case of pd scattering with only two possible inelastic pN collisions. If in the first collision a central mass M_1 is produced, in the second collision another central mass M_2 is produced and their rapidities overlap, then

it would not be possible to distinguish such an event from a single pN collision with the mass $M_1 + M_2$ produced in the center. Therefore hadron-nucleus and nucleus-nucleus collisions, rigorously speaking, only give information on the events with two fixed rapidity gaps, without specifying the exact nature of the object produced in between.

However the situation improves if one takes into account that the CD events have a very small probability, so that the described event with two central masses produced is highly improbable. Then the typical CD event will be that the central mass is produced in only one of the inelastic collisions, all others belonging to elastic or low mass diffractive events. In such a case the M_{cd} -dependence of the CD cross section will evidently repeat that for pp collisions.

An appropriate tool to calculate the CD cross section in hadron-nucleus and nucleus collisions is the so-called "criterion C " [58, 59, 60, 61]. It has been known since long ago that in the Glauber model the inelastic cross section is screened only by itself. As it turns out, there are many other types of events which are screened by themselves. These events have to possess a certain property C which satisfies the following requirement: Any superposition of NN events, in which at least one has property C , leads to the hA or AB event with property C . As a consequence, the only possibility to obtain an hA or AB event without property C should be that all NN events do not possess this property.

To translate the criterion C into formulas, let $\sigma_{AB}^{in}(\sigma)$ be the inelastic nucleus A -nucleus B cross section considered as a function of the total nucleon-nucleon cross section σ . Then the criterion C tells that for the events with the property C

$$\sigma_{AB}^c = \sigma_{AB}^{in}(\sigma^c) \quad (21)$$

which exactly means that they are shadowed only by themselves.

Passing to CD events, we have to apply the criterion C twice. First choose as events satisfying the criterion C those with particles produced at least in one of the two fixed rapidity gaps which determine the central region. Evidently any superposition of such NN events leads to an AB event of the same type. The complementary events are those in which no particle is produced in any of the two gaps. For NN collisions they include elastic events plus events in which particles are also produced in between the gaps and in the low mass diffractive regions of the projectile and target, above the upper gap and below the lower gap. Therefore the nucleon-nucleon cross section σ^c will be given by the difference

$$\sigma^c = \sigma - \sigma^{el} - \sigma^{lmd} - \sigma^{cd} \quad (22)$$

where σ^{lmd} refers to the mentioned low-mass diffractive contribution. σ^{cd} denotes the central diffraction contribution (to which also particles scattered elastically or low-mass diffraction contribute). Note that the magnitude of the low-mass diffractive part depends on the choice of the experimental setup which defines the events satisfying the criterion C . In particular, if these events are chosen to

include all low-mass diffractive contribution to the NN cross section, then the term σ^{lmd} will not appear in (22) and the cross section σ^{cd} will include only events with some particle produced in between the gap plus the projectile and target nucleons scattered elastically. In the following we shall be interested precisely in such CD events, having in mind that in the experimental setup for the photon-photon interaction small values of the momentum transferred to the colliding nuclei dominate, for which excitation of nucleon resonances is prohibited. For that reason we assume that all events with excitation of nucleon resonances are included in the events with the property C . Then (22) simplifies to

$$\sigma^c = \sigma^{in} - \sigma^{cd} \quad (23)$$

Subtracting from the total AB cross section the one with the described property C we find a cross section which is a sum of the elastic cross section, the cross section for the diffractive dissociation of the colliding nuclei and the CD cross section in which the nuclei either stay intact or are diffractively dissociated

$$\sigma_{AB}^{el} + \sigma_{AB}^{difd} + \sigma_{AB}^{cd} = \sigma_{AB}^{tot} - \sigma_{AB}^{in}(\sigma^{in} - \sigma^{cd}) \quad (24)$$

Now we repeat this argument taking for events satisfying C those in which any particle is produced in the whole rapidity range spanned by the two gaps and the rapidity interval in between. Such events also satisfy the conditions implied by the criterion C . The complementary events are now those in which no particle is produced in the described rapidity range at all. For NN collisions these are pure elastic events. For AB they also include nuclei diffraction dissociation events. Similar to (24) we then get the well known formula

$$\sigma_{AB}^{el} + \sigma_{AB}^{difd} = \sigma_{AB}^{tot} - \sigma_{AB}^{in}(\sigma^{in}) \quad (25)$$

Subtracting (25) from (24) we obtain the desired CD cross section for AB collisions

$$\sigma_{AB}^{cd} = \sigma_{AB}^{in}(\sigma^{in}) - \sigma_{AB}^{in}(\sigma^{in} - \sigma^{cd}) \quad (26)$$

This general formula can be written in an explicit form for hA collisions where the explicit dependence $\sigma_{hA}^{in}(\sigma)$ is known. In the Glauber model, for fixed impact parameter B ,

$$\sigma_{hA}^{in}(\sigma) = 1 - (1 - \sigma T(B))^A \simeq 1 - \exp(-A\sigma T(B)) \quad (27)$$

where $T(B)$ is the nuclear profile function. We then find the CD cross section

$$\begin{aligned} \sigma_{hA}^{cd} &= (1 - (\sigma^{in} - \sigma^{cd})T(B))^A - (1 - \sigma^{in}T(B))^A \\ &\simeq \exp(-A\sigma^{in}T(B))(\exp(A\sigma^{cd}T(B)) - 1) \end{aligned} \quad (28)$$

From the derivation it is clear that this cross section refers to the total probability to produce some particles between the two gaps and does not specify the

particles energy M . However, as mentioned, we can make use of the fact that σ^{cd} is very small. Then one approximately finds from (28)

$$\begin{aligned}\sigma_{hA}^{cd} &\simeq \sigma^{cd} AT(B)(1 - \sigma^{in}T(B))^{A-1} \\ &\simeq \sigma^{cd} AT(B) \exp(-A\sigma^{in}T(B))\end{aligned}\quad (29)$$

This cross section is linear in σ^{cd} . Therefore we can easily find the distribution in M

$$\begin{aligned}\frac{d\sigma_{hA}^{cd}(M)}{dM} &= \frac{d\sigma^{cd}(M)}{dM} AT(B)(1 - \sigma^{in}T(B))^{A-1} \\ &\simeq \frac{d\sigma^{cd}(M)}{dM} AT(B) \exp(-A\sigma^{in}T(B))\end{aligned}\quad (30)$$

As we observe, the absorption factor is universal and does not depend on M .

The application of this formalism to nucleus-nucleus collisions is hampered by the absence of an explicit (and tractable) expression for $\sigma_{AB}^{in}(\sigma)$. We shall use the well-known optical approximation in which $\sigma_{AB}^{in}(\sigma)$ is given by the same formula (27) with $A \rightarrow AB$ and an effective profile function for the two colliding nuclei

$$T_{AB} = \int d^2 B_1 T_A(B_1) T_B(B - B_1) \quad (31)$$

where B_1 is the usual two dimensional impact parameter. Our final formula for the CD cross section in AA collisions then follows from (30)

$$\frac{d\sigma_{AA}^{cd}(M)}{dM} = \frac{d\sigma^{cd}(M)}{dM} A_{\text{eff}}^2 \quad (32)$$

where A_{eff}^2 is the "effective" atomic number of the colliding nuclei defined by

$$A_{\text{eff}}^2 = A^2 \int d^2 B T_{AA}(B) \exp(-A^2 \sigma^{in} T_{AA}(B)) \quad (33)$$

We compute A_{eff}^2 using Woods-Saxon nuclear densities

$$\rho(r) = \frac{\rho_0}{1 + e^{(r-r_0)/a}} \quad (34)$$

with the standard parameter values [62] $r_0 = 1.14 A^{1/3}$ fm and $a = 0.545$ fm and and $\sigma^{in} = 73$ mb, as predicted in [29] for $\sqrt{s} = 6$ TeV. The values of A_{eff}^2 are given in Table 1 .

One observes that they are much smaller than A^2 . Actually $A_{\text{eff}}^2 \sim A^{1/3}$, so that even for very heavy colliding nuclei the CD cross section is only an order of magnitude greater than for proton-proton collisions.

2.3.2 Single diffraction cross sections in hadron-nucleus and photon-nucleus collisions

The derivation given above can be applied also to single diffraction with only one rapidity gap from the projectile or target side. One only has to appropriately change the events satisfying the criterion C . Then, instead of the central diffractive nucleon-nucleon cross section σ^{cd} in Eqs. (22) – (30) and (32), the corresponding single diffractive cross sections σ^d will appear. In particular, the final result for the nucleus-nucleus single diffractive cross section will be

$$\sigma_{AB}^d = \sigma_{AB}^{in}(\sigma^{in}) - \sigma_{AB}^{in}(\sigma^{in} - \sigma^d) \quad (35)$$

For hA collisions we obtain instead of (28) and (29)

$$\begin{aligned} \sigma_{hA}^d &= \exp(-A\sigma^{in}T(B))(\exp(A\sigma^dT(B) - 1)) \\ &\simeq \sigma^d AT(B) \exp(-A\sigma^{in}T(B)) \end{aligned} \quad (36)$$

and an analogous formula for $d\sigma_{hA}^d/dM^2$ similar to (30).

All of these formulae can be applied also for γP interactions in heavy ion collisions.

The final formula for γA diffractive scattering is similar to (32)

$$\frac{d\sigma_{\gamma A}^d(M)}{dM} = \frac{d\sigma_{\gamma h}^d(M)}{dM} A_{\text{eff}} \quad (37)$$

with

$$A_{\text{eff}} = A \int d^2B T_A(B) \exp(-A\sigma^{in}T_A(B)) \quad (38)$$

We calculate A_{eff} with the same input as for A_{eff}^2 in Eq. (33) and present the values also in Table 1. Actually also $A_{\text{eff}} \sim A^{1/3}$, this is a behaviour found before by Ranft and Roesler [63] and by Faessler [64].

3 Comparing hadronic photon-photon interactions with diffractive interactions in heavy ion collisions

3.1 Cross sections

We calculate the cross sections $d\sigma/dM_X$ for the production of a central cluster of hadrons with invariant mass M_X . This is done for proton-proton collisions as well as for symmetrical heavy ion collisions with the same projectile and target ion. The calculations are done for light (O), medium (Ca, Fe, Ag) and heavy ions (Pb) with the energies of the future LHC hadron and heavy ion collider

under construction at CERN. The two ions most likely to be used in the LHC experiments [12] are Pb for obtaining the highest energy densities and Ca, where a larger luminosity than with Pb can be obtained. It was shown [65] that the luminosity in Ca-Ca collisions could be up to a factor 10^4 larger than in Pb-Pb collisions. This gain more than compensates the loss in the two-photon flux in the Ca-Ca reaction. ($L_{\text{Pb-Pb}} \approx 5 \times 10^{26} \text{ cm}^{-2}\text{s}^{-1}$, $L_{\text{Ca-Ca}} \approx 5 \times 10^{30} \text{ cm}^{-2}\text{s}^{-1}$).

For photon-photon collisions we use two different approaches for calculating photon fluxes described in the Appendix. These two approximations give slightly different cross sections especially at large masses M_X .

In Figs. 4–9 we compare the cross section for the production of a hadronic cluster of invariant mass M_X in photon-photon collisions with the corresponding cross section for the double-pomeron and photon-pomeron reactions. The calculation was done for pp collisions and for heavy ion collisions O-O, Ca-Ca, Fe-Fe, Ag-Ag, and Pb-Pb at the energy of the LHC ($\sqrt{s} = 6 \text{ A TeV}$). For the photon-photon collisions we show the results using the form factor approximation (F) and the semi-classical, geometric approximation (G) to calculate the heavy ion photon flux. For the Pb-Pb reaction we use in fact two different form factors, (F) the geometric approximation to the form factor (see Eq. (47)) and (FF), the Gaussian approximation. Both approximations lead to nearly identical cross sections $d\sigma/dM_X$, therefore, we present for all other reactions only the (F) cross section. The double-pomeron cross sections are given for three different kinematical cuts ($M_{cd} > 2 \text{ GeV}/c^2$, $c = 0.90, 0.95$ and 0.97). The photon-pomeron cross sections are given for only one setting of the kinematical cuts ($M_{\gamma P} > 2 \text{ GeV}/c^2$ and $c = 0.95$). Of course, these cuts depend on the experimental setup of such an experiment, which is not known at present, but any cuts are easy to apply to our Monte Carlo events.

Even given the considerable uncertainty in the cross sections for CD and photon-pomeron collisions, the conclusions from Figs. 4–9 are rather obvious. The study of the pure two-photon reaction without background from central diffraction and photon-pomeron collisions is not possible. In proton-proton collisions and collisions of light and medium heavy ions the central diffraction reaction dominates. For heavy ion collisions the photon-pomeron cross section is comparable to the photon-photon cross section. Many interesting particles might be produced and studied in photon-photon photon-pomeron as well as pomeron-pomeron collisions. If a reaction is to be studied using pomeron-pomeron collisions, then the best results should be obtained in pp collisions, where the highest luminosity can be obtained.

3.2 Rapidity distributions

In order to demonstrate that the three reactions studied lead to very similar signatures of the events we present in Fig. 10 pseudorapidity distributions of the produced hadrons. The Figure shows the distribution of hadrons in photon-

photon reactions in Pb-Pb and Ca-Ca heavy ion collisions (only the hadrons produced in the central cluster of particles are included in the histogram). The distribution in CD are presented for pp collisions and in this case we include also the scattered incoming protons into the histogram. The distribution for photon-pomeron collisions is presented for Pb-Pb collisions and includes only the hadrons from the central cluster.

With the photon fluxes used and with the kinematical cuts for the diffractive reactions, we obtain in all cases two large rapidity gaps between the central cluster of hadrons and the scattered original protons or heavy ions. The distributions given in Fig. 10 represent the average pseudorapidity distributions averaged over many collisions and the mass spectrum given in Figs. 4 to 9. In each single event the pseudorapidity distribution corresponding to the central cluster will be less wide than the average and it will in general not be in the center of the nucleon-nucleon CMS.

4 Conclusions and summary

Photon-photon collisions as well as central diffraction and photon-pomeron collisions are very interesting reaction channels at proton-proton and heavy ion colliders in the TeV energy range.

Here we compare the cross sections of the three channels for the production of hadronic systems of given invariant mass M_X . The three reaction channels have very similar experimental signatures, a central cluster of produced particles and two large rapidity gaps.

The cross section for CD and photon-pomeron collisions is still subject to large uncertainties (as large as a factor of three) in the TeV energy region.

We find for proton-proton and light up to medium-heavy ion reactions that the central diffraction cross section dominates the two photon and photon-pomeron cross sections. In collisions of the heaviest ions like Pb-Pb the photon-pomeron channel and the photon-photon channel are of comparable magnitude, however at very large masses CD can be larger than the other two channels depending on the experimental cuts.

The conclusion is obvious. Central double-pomeron processes are best studied in pp collisions, where the largest luminosities are obtained, this compensates the rise of the double-pomeron cross section in heavy ion reactions. If photon-photon reactions are to be studied, then it should be the best to use the heaviest ions available at future colliders but even then the background from photon-pomeron collisions will be roughly of the same size as the signal.

Acknowledgements

Discussions with K. Eggert and S. Roesler are gratefully acknowledged. The

authors thank K. Hencken for providing them the code [5] to calculate photon fluxes in heavy ion collisions using the semi-classical approximation. One of the authors (R.E.) was supported by the Deutsche Forschungsgemeinschaft under contract No. Schi 422/1-2. One of the authors (J.R.) was supported by the Direccion General de Politicia Cientifica of Spain.

A Appendix:Photon flux calculation

It is convenient to define the luminosity function for the photon flux in hadron-hadron scattering by

$$\frac{dL}{dy_1 dP_1^2 dy_2 dP_2^2} = f(y_1, p_1^2; y_2, p_2^2) \Theta(s_{1,2} - s_{\min}). \quad (39)$$

Here, p_1 and p_2 are the four momenta of the photons forming the subsystem. $p_1^2 = -P_1^2$ and $p_2^2 = -P_2^2$ are the photon virtualities. The variables y_1 and y_2 denote approximately the energy fractions taken by the photons from the initial hadrons as explained below. The Heavyside function in (39) restricts the invariant mass of the system formed by the four momenta p_1 and p_2 to allow the application of the model. To obtain the cross sections for the processes mentioned above, the luminosity function is folded with the $\gamma\gamma$ cross section.

As a first step, photon emission off a pointlike particle is discussed using as example the kinematics of ep scattering, shown in Fig. 11. To characterize deep-inelastic scattering, we use the variables x and y

$$x = \frac{P^2}{2(p_p \cdot p)} \quad y = \frac{(p \cdot p_p)}{(p_e \cdot p_p)} \quad (40)$$

where x denotes Bjorken's scaling variable. Then, the differential cross section for ep scattering via photon exchange can be written in terms of the structure functions $F_1(x, P^2)$ and $F_2(x, P^2)$

$$\begin{aligned} \frac{d\sigma^{ep}}{dy dP^2} &= \frac{4\pi\alpha_{\text{em}}^2}{P^4} \left\{ xy \left(1 - \frac{2m_e^2}{P^2} \right) F_1(x, P^2) \right. \\ &\quad \left. + \frac{1}{y} \left(1 - y - \frac{m_p^2 P^2}{((p_e \cdot p_p)^2 - m_e^2 - m_p^2)^2} \right) F_2(x, P^2) \right\}. \end{aligned} \quad (41)$$

Here, α_{em} denotes the fine structure constant and m_e is the electron mass. In the limit of high collision energies, terms proportional to $m_p^2/(p_e \cdot p_p)^2$ and $m_e^2/(p_e \cdot p_p)^2$ can be neglected. Using the optical theorem, the structure functions can be related to the total γp cross sections for virtual photons with transverse polarization

(helicity ± 1) $\sigma_T^{\gamma p}$ and scalar polarization (helicity 0) $\sigma_S^{\gamma p}$ [66]

$$F_1(x, P^2) = \frac{(p_p \cdot p)(1-x)}{8\pi^2 \alpha_{\text{em}}} \sigma_T^{\gamma p} \quad (42)$$

$$F_2(x, P^2) = 2 \frac{P^2(1-x)(\sigma_T^{\gamma p} + \sigma_S^{\gamma p})}{8\pi^2 \alpha_{\text{em}}(1 - m_p^2 P^2 / (p_p \cdot p))} . \quad (43)$$

For small values of P^2 , (41) simplifies to

$$\frac{d\sigma^{ep}}{dy dP^2} = \frac{\alpha_{\text{em}}}{2\pi P^2} \left(\frac{1 + (1-y)^2}{y} - 2m_e^2 y \frac{1}{P^2} \right) \sigma_T^{\gamma p} . \quad (44)$$

It should be emphasized that in the high-energy limit the flux of weakly virtual photons can be factorized out and is independent of the second scattering particle, which allows to introduce the generic photon flux function for bremsstrahlung

$$f_{\gamma,e}(y, P^2) = \frac{\alpha_{\text{em}}}{2\pi P^2} \left(\frac{1 + (1-y)^2}{y} - 2m_e^2 y \frac{1}{P^2} \right) . \quad (45)$$

Due to the complex structure of the charge distribution $\rho(\vec{x})$ in hadrons, several approximations and assumptions are necessary to calculate the flux of weakly virtual photons. The approaches in literature can be subdivided into [67]: (i) methods using charge form factors for the hadrons [2, 6] and (ii) methods using the semi-classical methods and geometrical interpretations on the basis of the impact parameter representation (for example [3, 1, 68, 5]).

In the form factor approach, Eq. (45) can be used directly. The effects due to the finite charge space-distribution can be included by substituting

$$\alpha_{\text{em}} \longrightarrow Z^2 \alpha_{\text{em}} |F(p^2)|^2 \quad (46)$$

for each colliding hadron where Z denotes the electric charge number. The weak point on this approach are the almost unknown elastic form factors $F(p^2)$ for heavy ions. The simplest assumption for the heavy ion elastic form factor is motivated by the geometrical interpretation: In the classical picture one should only consider photons having an impact parameter \vec{B} relative to the hadron greater than the transverse hadron size $R \approx 1.2 \text{fm}$ $A^{1/3}$. With $P^2 \sim 1/\vec{B}^2$ follows

$$F(p^2) = \int d^3x \rho(\vec{x}) e^{i\vec{p}\cdot\vec{x}} = \begin{cases} 1, & -p^2 < 1/R^2 \\ 0, & -p^2 \geq 1/R^2 \end{cases} \quad (47)$$

More realistic parametrizations of the elastic form factor can be found in literature [69]. For example, the form factor of ^{206}Pb can be parametrized by a Gaussian distribution $F(p^2) = \exp(p^2/Q_0^2)$ with $Q_0 \approx 55 - 60 \text{ MeV}$ as used in Ref. [6].

The basis of the semi-classical (geometrical) methods is the fact that a fast-moving charged particle develops a magnetic field almost of the same size as the

electric field. This can be described by photons moving parallel to the particle at an impact parameter \vec{B} (see Fig 12).

The number of equivalent photons is given by [70]

$$f(y, \vec{B}) = \frac{Z^2 \alpha_{\text{em}}}{\pi^2} (my)^2 \frac{1}{y} \left[K_1^2(m|\vec{B}|y) + \frac{m^2}{E^2} K_0^2(m|\vec{B}|y) \right], \quad (48)$$

where K_0 and K_1 denote the modified Bessel functions, E and m are the energy and the mass of the hadron (heavy ion), respectively. Since the virtualities of the photons are neglected, the photon energy is given directly by $\omega = yE$. For elastic heavy ion scattering, the impact parameter of the equivalent photons is restricted to $|\vec{B}| > R$. The total photon flux follows from

$$\begin{aligned} f(y) &= 2\pi \int_R^\infty f(y, \vec{B}) B dB \\ &= \frac{2}{y} \frac{Z^2 \alpha_{\text{em}}}{\pi} \left[\xi K_0(\xi) K_1(\xi) - \frac{\xi^2}{2} (K_1^2(\xi) - K_0^2(\xi)) \right] \end{aligned} \quad (49)$$

$$(50)$$

with $\xi = mRy$. The transverse distance between the particles should be larger than the transverse sizes of the particles to make sure that the particles do not interact hadronically which leads to the luminosity function [3, 68, 5]

$$\begin{aligned} \frac{dL}{dy_1 dy_2} &= \int_{|\vec{B}_1| > R_1} \int_{|\vec{B}_2| > R_2} f(y_1, \vec{B}_1) f(y_2, \vec{B}_2) \\ &\quad \times \Theta(s_{1,2} - s_{\text{min}}) \Theta(|\vec{B}_1 - \vec{B}_2| - (R_1 + R_2)) d^2 B_1 d^2 B_2 . \end{aligned} \quad (51)$$

In the case of photon-pomeron scattering one has to consider photon-hadron (photon-heavy ion) scattering. The flux function reads (for example, for the electromagnetic interaction of particle B)

$$\frac{dL}{dy_2} = \int_{|\vec{B}_2| > R} f(y_2, \vec{B}_2) \Theta(s_{1,2} - s_{\text{min}}) . \quad (52)$$

Here, the radius R is the minimum impact parameter of the photon that the heavy ions do not overlap in transverse space as shown in Fig. 13. A value of $R = R_1 + R_2$ would satisfy this condition, however, since diffractive processes are mainly peripheral processes [64], there may be also contributions with $R_2 < |\vec{B}| < R_1 + R_2$. The results shown here were obtained using $R = R_1 + R_2$. Lowering the impact parameter cutoff to $R = R_2$ increases the photon flux approximately by 20%.

References

- [1] C. A. Bertulani and G. Baur: Phys. Rep. 163 (1988) 181
- [2] M. Grabiak, B. Müller, W. Greiner, G. Soff and P. Koch: J. Phys. G15 (1989) L25
- [3] E. Papageorgiu: Phys. Lett. B250 (1990) 155
- [4] M. Vidović, M. Greiner, C. Best and G. Soff: Phys. Rev. C47 (1993) 2308
- [5] K. Hencken, D. Trautmann and G. Baur: Z. Phys. C68 (1995) 473
- [6] M. Drees, J. Ellis and D. Zeppenfeld: Phys. Lett. B223 (1989) 454
- [7] E. Papageorgiu: Phys. Rev. D40 (1989) 92
- [8] M. Greiner, M. Vidović, J. Rau and G. Soff: J. Phys. G17 (1991) L45
- [9] M. Greiner, M. Vidović and G. Soff: Phys. Rev. C47 (1993) 2288
- [10] E. Papageorgiu: Phys. Lett. B352 (1995) 394
- [11] J. Ohnemus, T. F. Walsh and P. M. Zerwas: Phys. Lett. B328 (1994) 369
- [12] ALICE Collaboration: ALICE technical proposal, CERN report CERN/LHCC/95-71, 1995
- [13] G. Ingelman and P. E. Schlein: Phys. Lett. B152 (1985) 256
- [14] UA8 Collab.: R. Bonino et al.: Phys. Lett. B211 (1988) 239
- [15] UA8 Collab.: A. Brandt et al.: Phys. Lett. B297 (1992) 417
- [16] A. Schaefer, O. Nachtman and R. Schoepf: Phys. Lett. B249 (1990) 331
- [17] A. Bialas and P. V. Landshoff: Phys. Lett. B256 (1991) 540
- [18] R. S. Fletcher and T. Stelzer: Phys. Rev. D48 (1993) 5163
- [19] J. Ellis and P. Salati: CERN Report CERN TH-5693, 1990
- [20] K. H. Streng: Phys. Lett. 166B (1986) 443
- [21] A. Bialas and W. Szeremeta: Phys. Lett. B296 (1992) 191
- [22] A. Bialas and R. Janik: Z. Phys. C62 (1994) 487
- [23] M. Heyssler: Diffractive heavy flavor production at the TEVATRON and the LHC, DTP/96/10, 1996

- [24] A. A. Natale: Mod. Phys. Lett. A22 (1994) 2075
- [25] A. A. Natale: Phys. Lett. B362 (1995) 177
- [26] A. Capella, J. Tran Thanh Van and J. Kwiecinski: Phys. Rev. Lett. 58 (1987) 2015
- [27] P. Aurenche, F. W. Bopp, A. Capella, J. Kwiecinski, M. Maire, J. Ranft and J. Tran Thanh Van: Phys. Rev. D45 (1992) 92
- [28] F. W. Bopp, R. Engel, D. Pertermann and J. Ranft: Phys. Rev. D49 (1994) 3236
- [29] R. Engel: Z. Phys. C66 (1995) 203
- [30] R. Engel and J. Ranft: Hadronic photon-photon collisions at high energies, preprint ENSLAPP-A-540/95, (hep-ph/9509373), 1995
- [31] R. Engel, J. Ranft and S. Roesler: Phys. Rev. D52 (1995) 1459
- [32] R. Engel and J. Ranft: to be published, 1996
- [33] P. Aurenche, F. W. Bopp, R. Engel, D. Pertermann, J. Ranft and S. Roesler: Comp. Phys. Commun. 83 (1994) 107
- [34] R. Engel: Photoproduction within the Dual Parton Model, Talk given at XXIXth Rencontre de Moriond, in Proceedings of the XXIXth Rencontre de Moriond, Page 321, ed. by J. Trân Thanh Vân, Edition Frontieres, Gif-sur-Yvette, 1994
- [35] R. Engel: Multiparticle Photoproduction within the two-component Dual Parton Model, in preparation, 1996
- [36] M. Glück, E. Reya and A. Vogt: Phys. Rev. D45 (1992) 3986
- [37] M. Glück, E. Reya and A. Vogt: Phys. Rev. D46 (1992) 1973
- [38] V. A. Abramovski, V. N. Gribov and O. V. Kancheli: Yad. Fis. 18 (1973) 595
- [39] K. A. Ter-Martirosyan: Phys. Lett. B44 (1973) 377
- [40] K. Hahn and J. Ranft: Phys. Rev. D41 (1990) 1463
- [41] A. Capella, U. Sukhatme, C. I. Tan and J. Tran Thanh Van: Z. Phys. C10 (1980) 249
- [42] A. B. Kaidalov: Phys. Lett. B116 (1982) 459

- [43] A. Capella, A. Kaidalov, C. Merino, D. Pertermann and J. Tran Thanh Van: Phys. Rev. D53 (1996) 2309
- [44] H. U. Bengtsson and T. Sjöstrand: Comp. Phys. Commun. 46 (1987) 43
- [45] M. L. Good and W. D. Walker: Phys. Rep. 120 (1960) 1854
- [46] A. B. Kaidalov: Phys. Rep. 50 (1979) 157
- [47] S. Roesler, R. Engel and J. Ranft: Z. Phys. C59 (1993) 481
- [48] A. Capella and J. Kaplan: Phys. Lett. B52 (1974) 448
- [49] A. Capella, J. Kaplan and J. Tran Thanh Van: Nucl. Phys. B105 (1976) 333
- [50] E. Gotsman, E. M. Levin and U. Maor: Phys. Rev. D49 (1994) 4321
- [51] H1 Collab.: S. Aid et al.: Z. Phys. C69 (1995) 27
- [52] D. M. Chew and G. F. Chew: Phys. Lett. 53B (1974) 191
- [53] A. B. Kaidalov and K. A. Ter-Martirosyan: Nucl. Phys. B75 (1974) 471
- [54] A. Berera and J. C. Collins: Double pomeron jet cross sections, report PSU/TH/162, (hep-ph/9509258), 1995
- [55] J. Pumplin: Phys. Rev. D47 (1993) 4820
- [56] E. Gotsman, E. M. Levin and U. Maor: Phys. Lett. B353 (1995) 526
- [57] N. Armesto and M. A. Braun: The pomeron-pomeron interaction in the perturbative QCD, preprint US-FT/27-96, (hep-ph/9606307), 1996
- [58] A. Blankenbecler, A. Capella, J. Tran Thanh Van, C. Pajares and V. A. Ramallo: Phys. Lett. B 107 (1981) 106
- [59] C. Pajares and V. A. Ramallo: Phys. Lett. B107 (1981) 238
- [60] C. Pajares and V. A. Ramallo: Phys. Rev. D31 (1985) 2800
- [61] M. A. Braun and C. Pajares: Nucl. Phys. A532 (1991) 678
- [62] E. Segré: *Nuclei and particles* Reading Mass Benjamin 1977
- [63] J. Ranft and S. Roesler: Z. Phys. C62 (1994) 329
- [64] M. A. Faessler: Z. Phys. C58 (1993) 567
- [65] D. Brandt, K. Eggert and A. Morsch: CERN Report CERN AT/94-05, LHC Note 264, 1994

- [66] V. M. Budnev, I. F. Ginzburg, G. V. Meledin and V. G. Serbo: Phys. Rep. 15C (1975) 181
- [67] G. Baur and C. A. Bertulani: Z. Phys. A330 (1988) 77
- [68] N. Baron and G. Baur: Phys. Rev. C48 (1993) 1999
- [69] R. C. Barret and D. F. Jackson: *Nuclear size and structure* Clarendon Oxford 1977
- [70] J. D. Jackson: *Classical electrodynamics* John Wiley & Sons New York 1963

Table 1: Results for the effective A_{eff}^2 in AA collisions (second column) and the effective A -dependence in hA collisions (third column) using $\sigma_{in} = 73$ mb and Woods-Saxon nuclear densities.

Nucleus	A	A_{eff}^2	A_{eff}
O	16	4.94	2.36
Ca	40	6.21	2.92
Fe	56	6.76	3.16
Ag	108	8.00	3.71
Pb	208	9.52	4.39

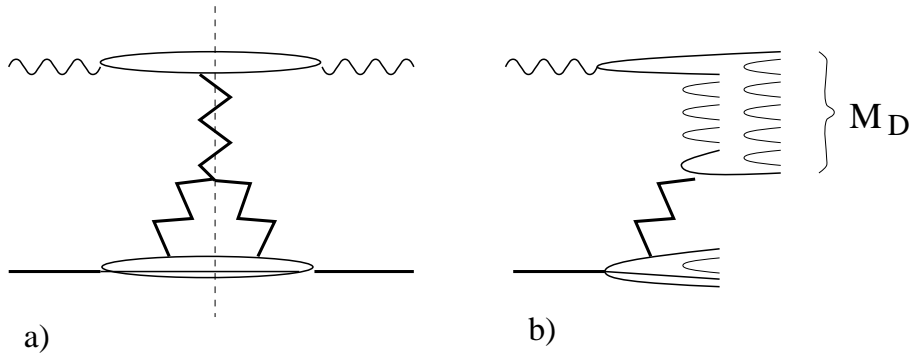


Figure 1: High-mass photon diffraction dissociation: diffractive cut of the triple-pomeron graph a) and the corresponding chain system b)

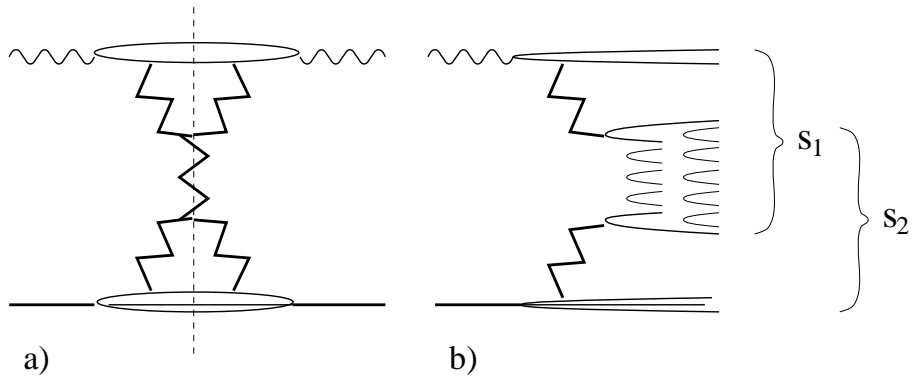


Figure 2: Central diffraction: diffractive cut of the double-pomeron graph a) and the corresponding chain system b).

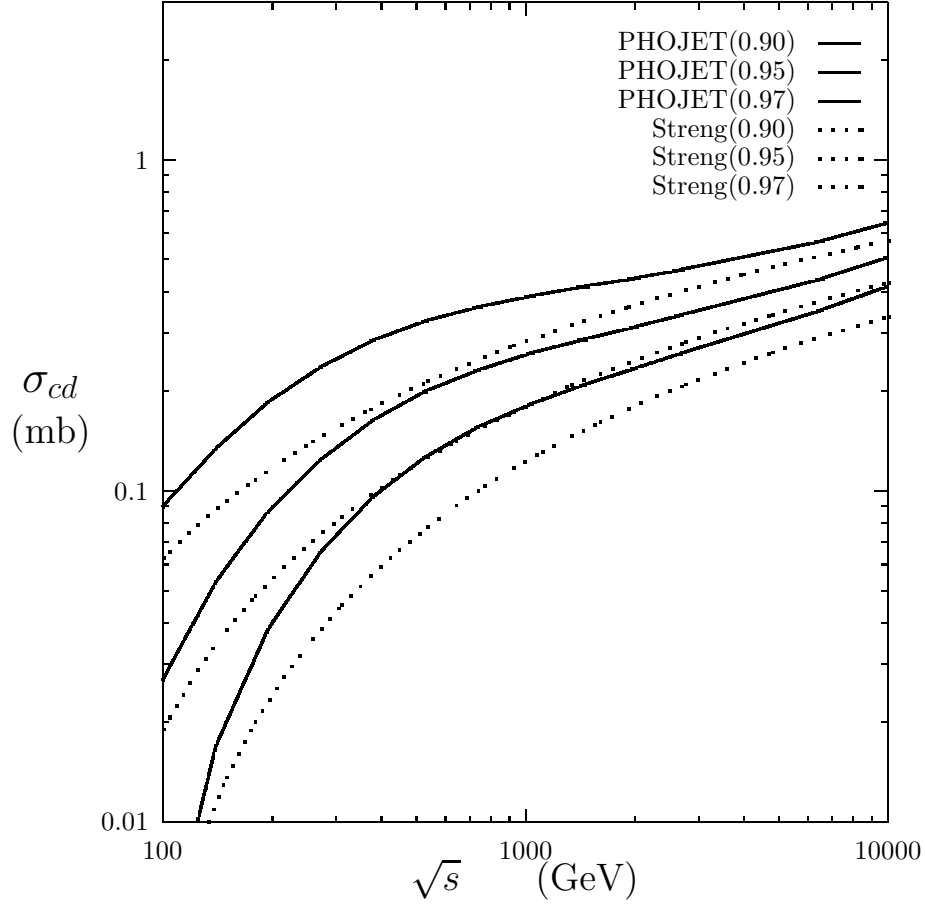


Figure 3: The energy dependence of the central diffraction cross section. We compare the cross section as obtained from PHOJET with unitarization using a supercritical pomeron with the cross section obtained by Streng [20] without unitarization and with a critical pomeron. Both cross sections are for the same three kinematical cuts: $M_{cd} > 2\text{GeV}/c^2$ and $c = 0.90, 0.95$ and 0.97 . Please note, to identify the cross sections, the cross sections decrease with rising c .

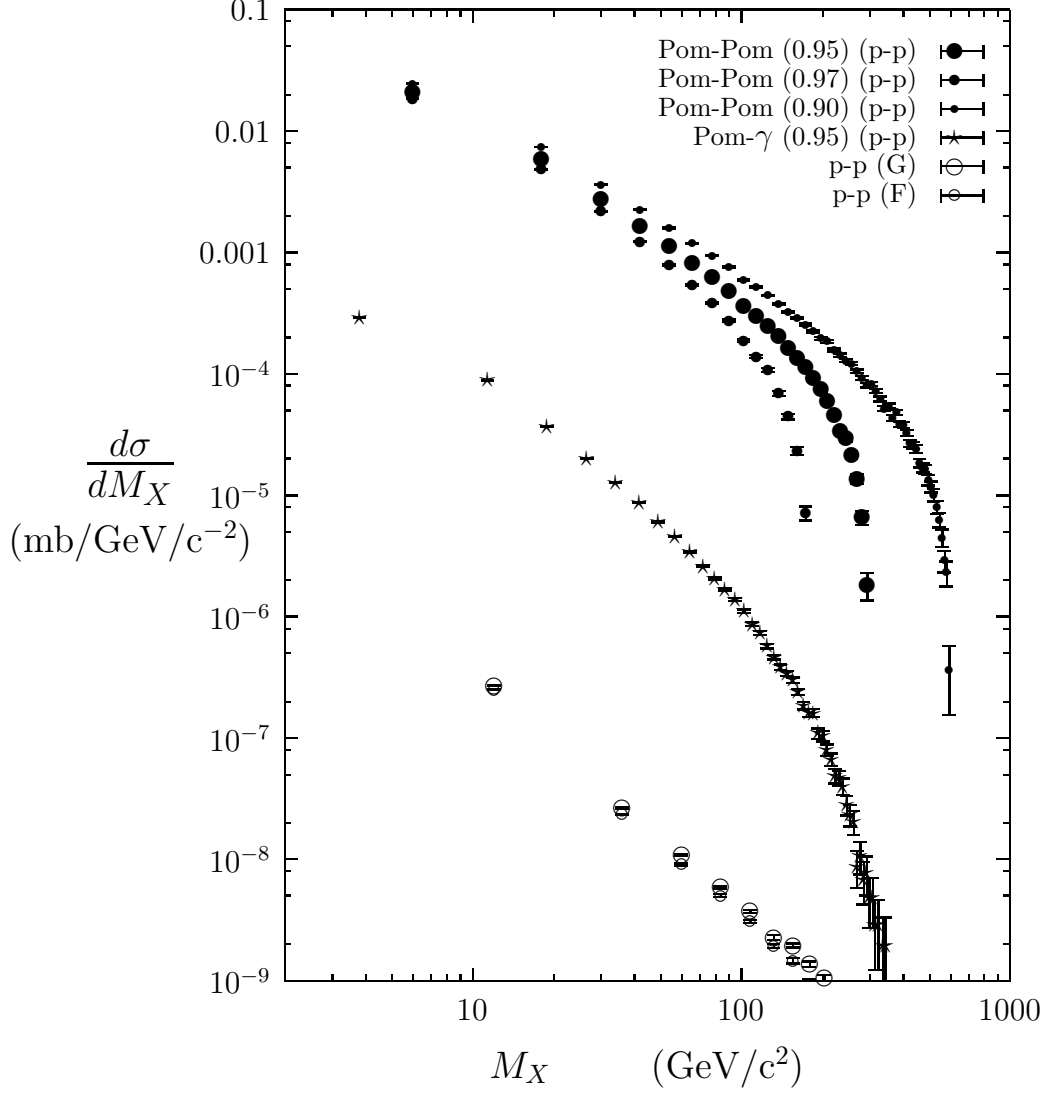


Figure 4: We compare the cross section for the production of a hadronic cluster of invariant mass M_X via photon-photon interaction in proton-proton collisions using two different methods (F) and (G) to calculate the photon flux, described in the Appendix with the corresponding cross section for the diffractive reactions. The central diffraction cross sections (pomeron-pomeron collisions) are given for three different kinematical cuts $M_{cd} > 2 \text{ GeV}/c^2$, $c = 0.90, 0.95$ and 0.97 . The single diffraction photon-pomeron cross section is given for $M_{\gamma P} > 2 \text{ GeV}/c^2$ and $c = 0.95$.

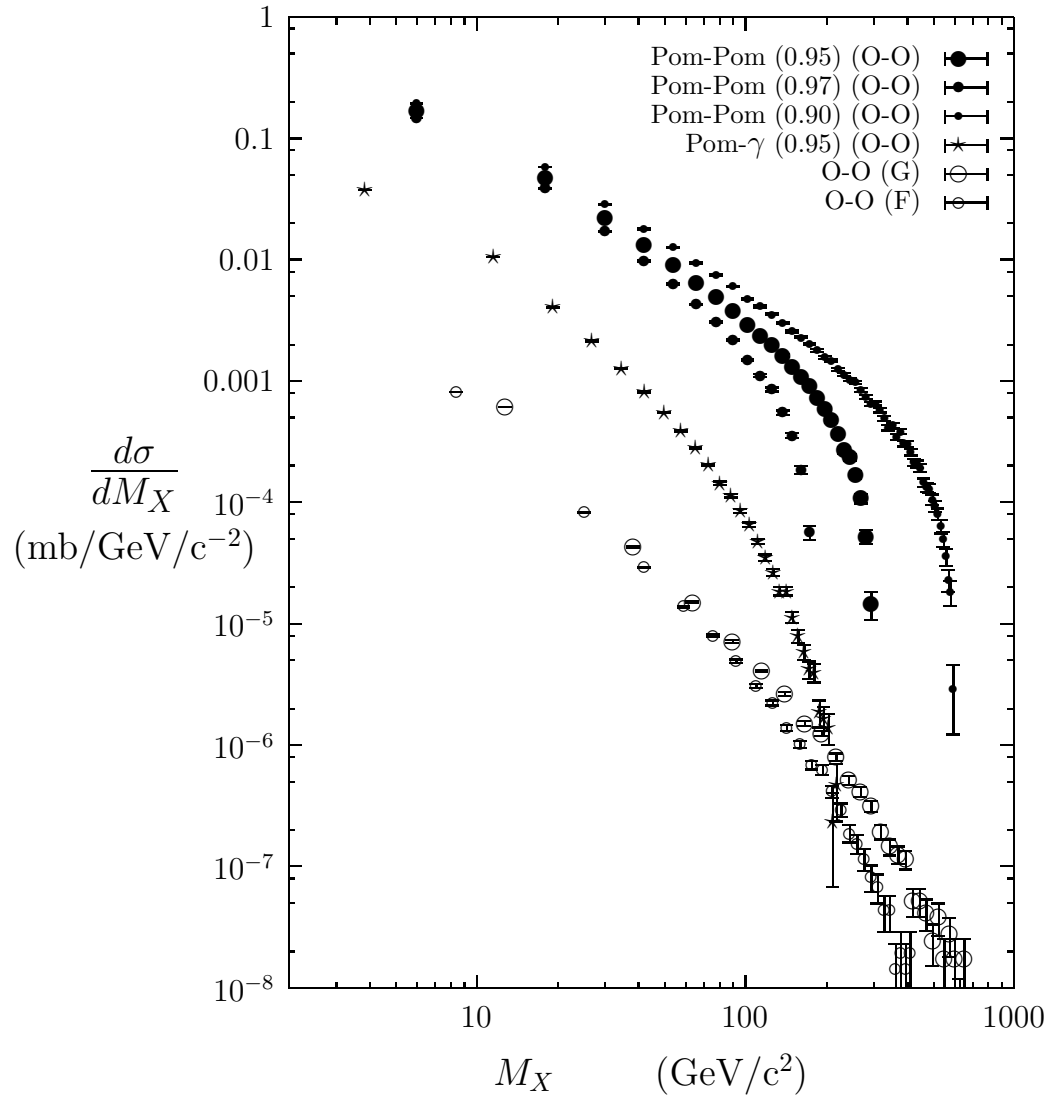


Figure 5: As Fig. 4 but for heavy ion reactions O-O.

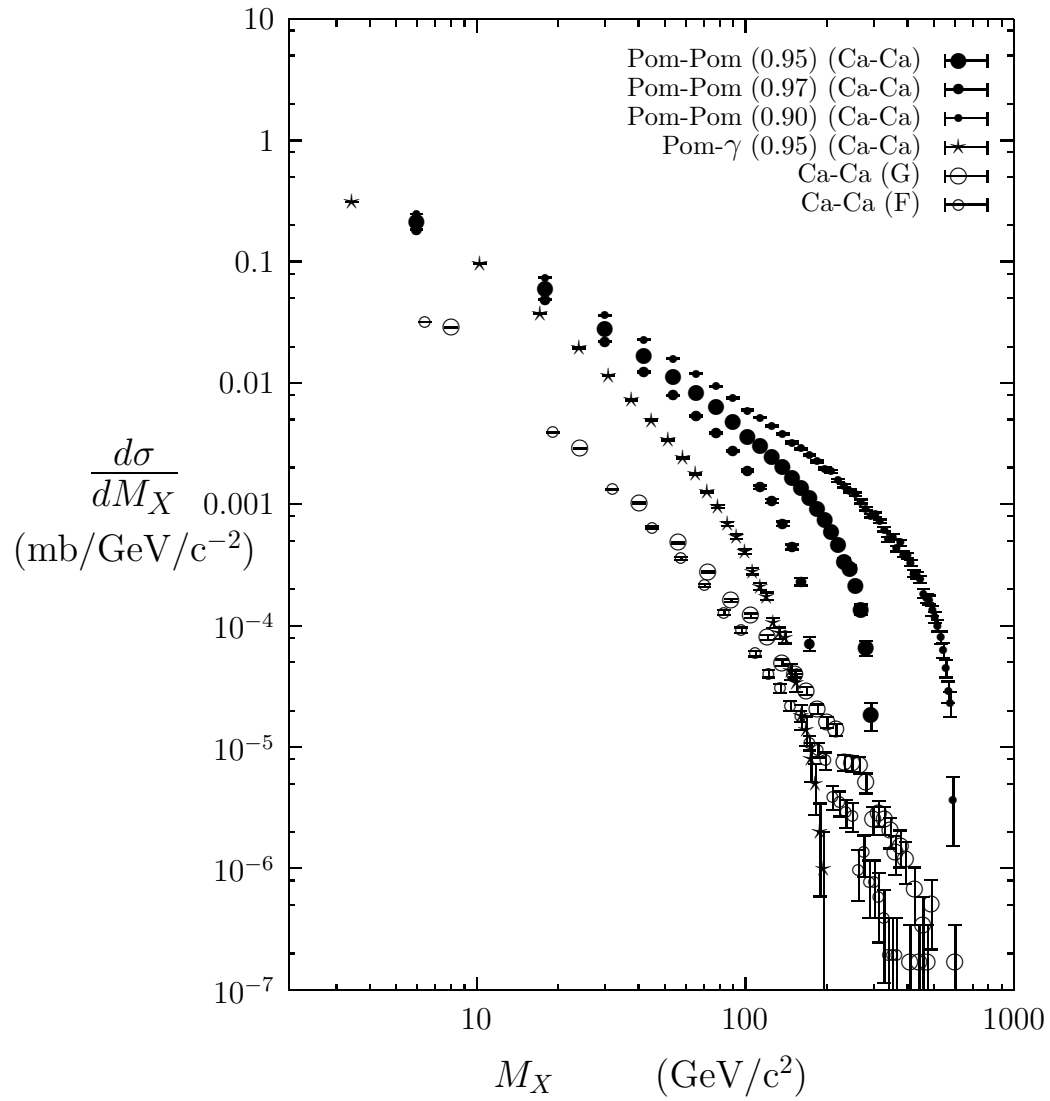


Figure 6: as Fig. 4 but for heavy ion reactions Ca-Ca.

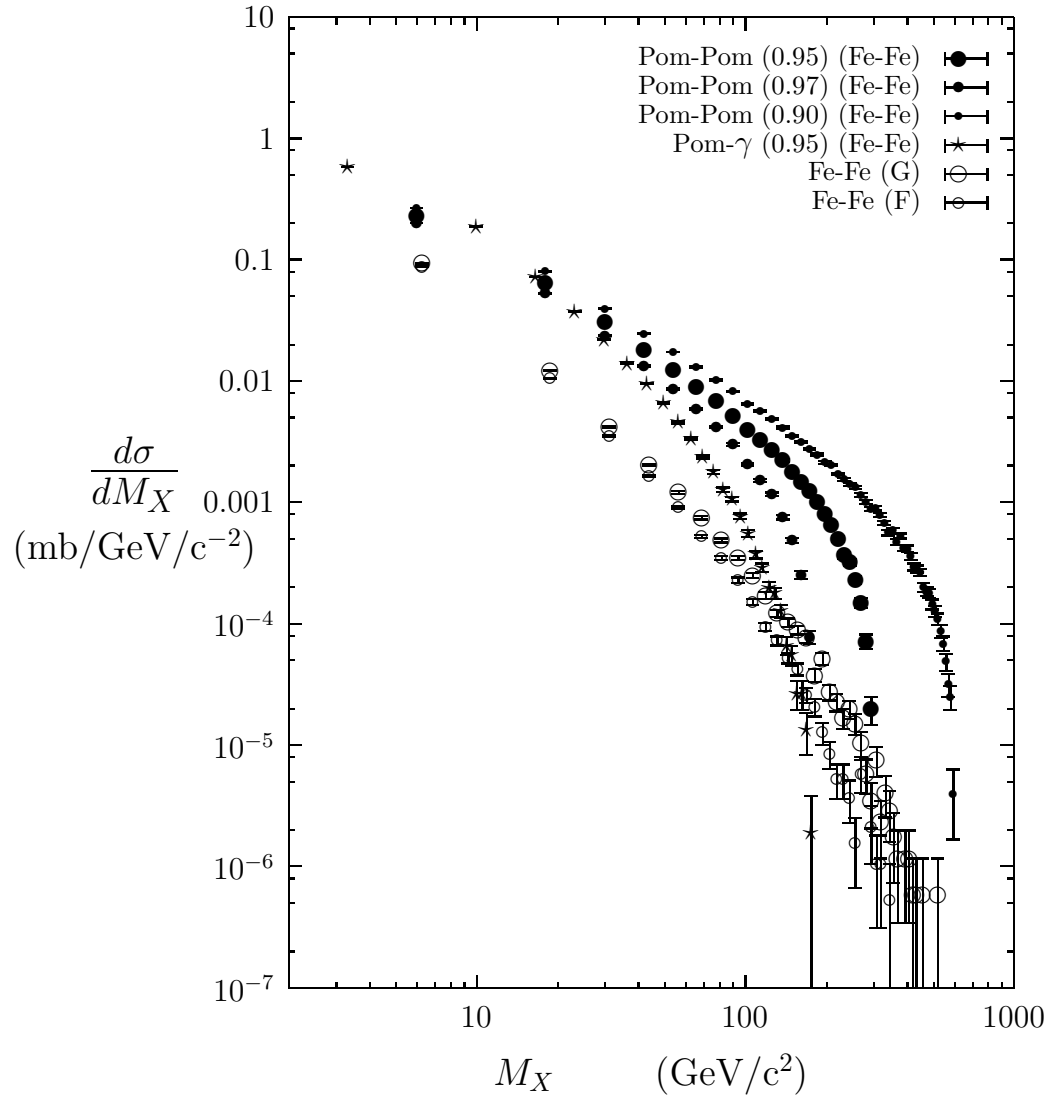


Figure 7: As Fig. 4 but for heavy ion reactions Fe-Fe.

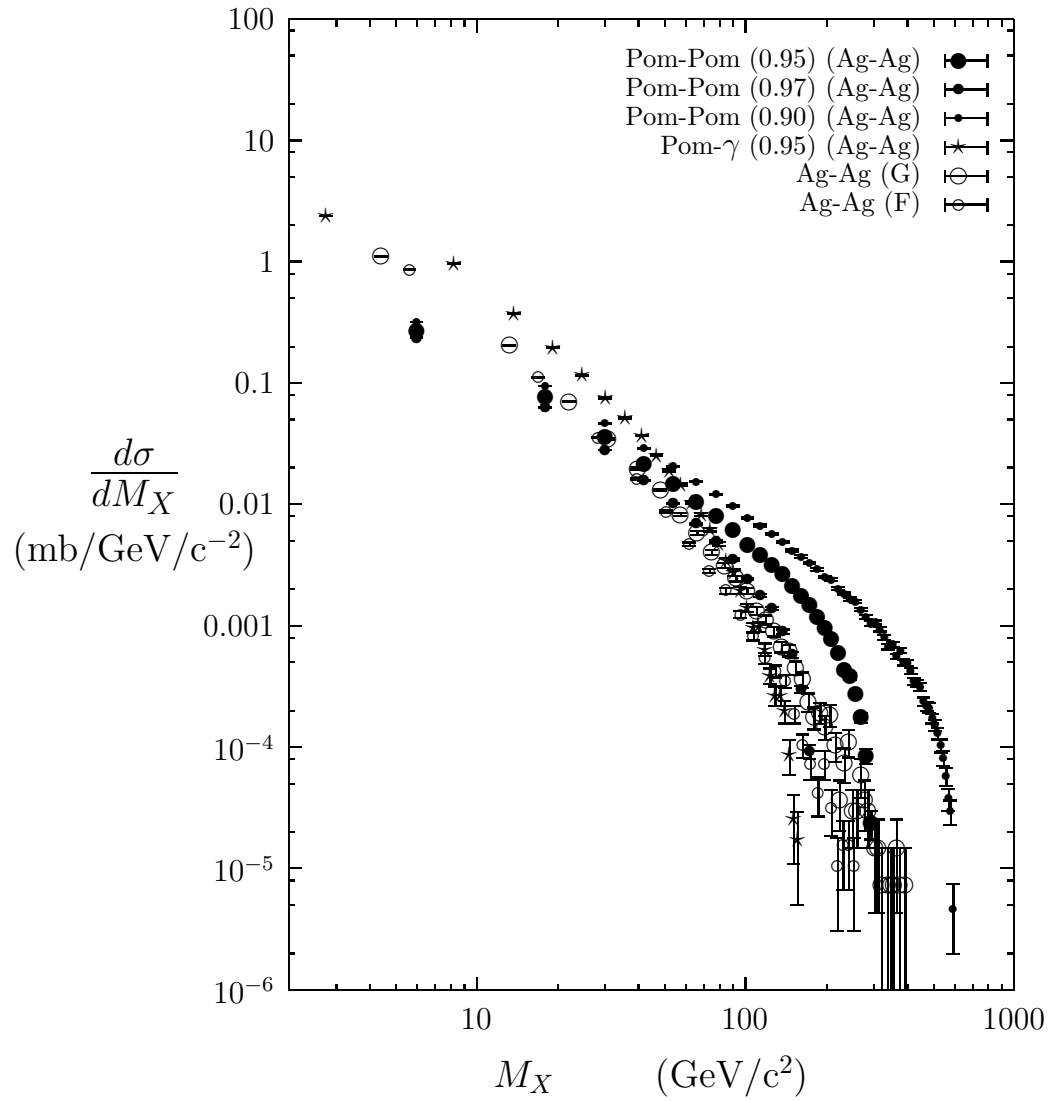


Figure 8: As Fig. 4 but for heavy ion reactions Ag-Ag.

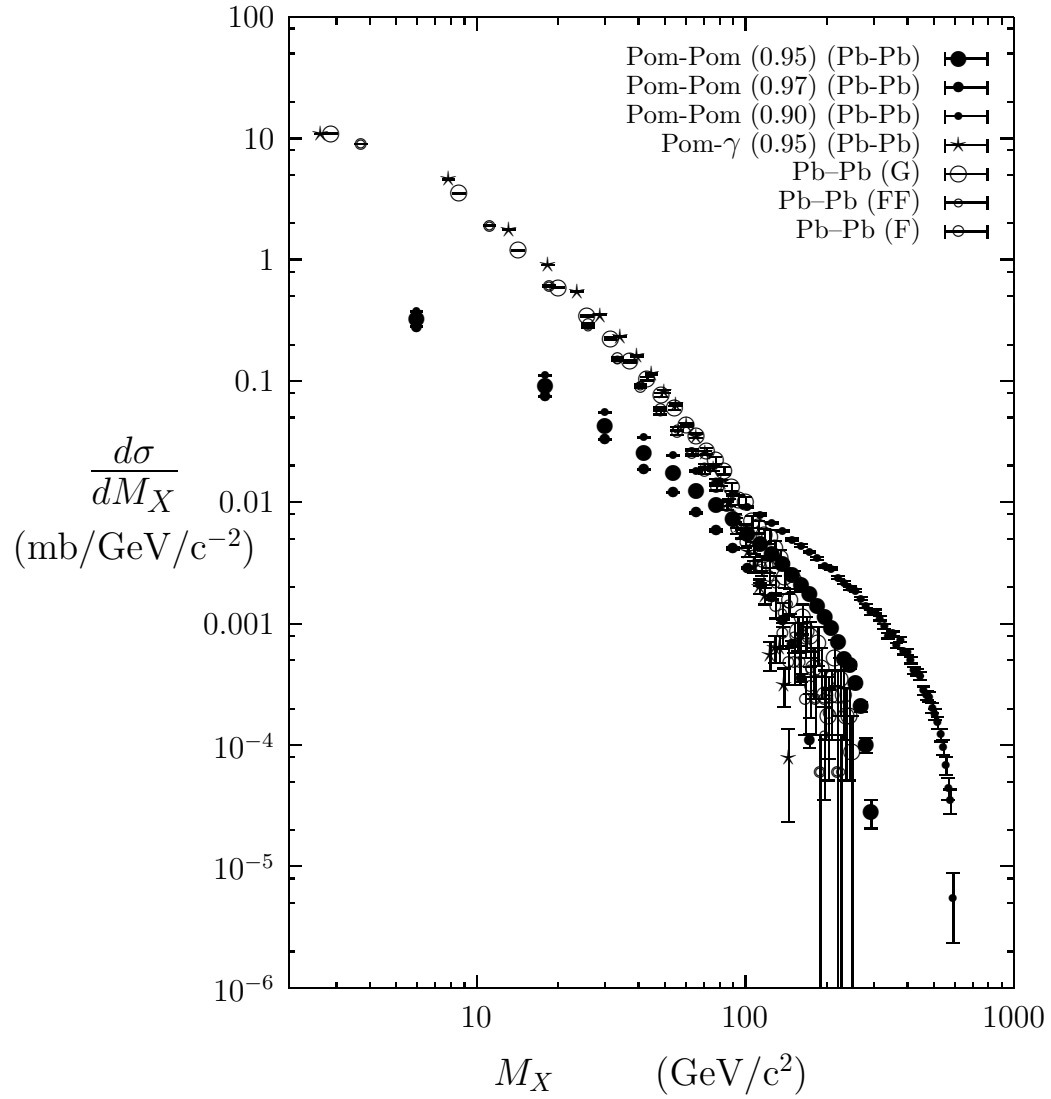


Figure 9: As Fig. 4 but for heavy ion reactions Pb-Pb.

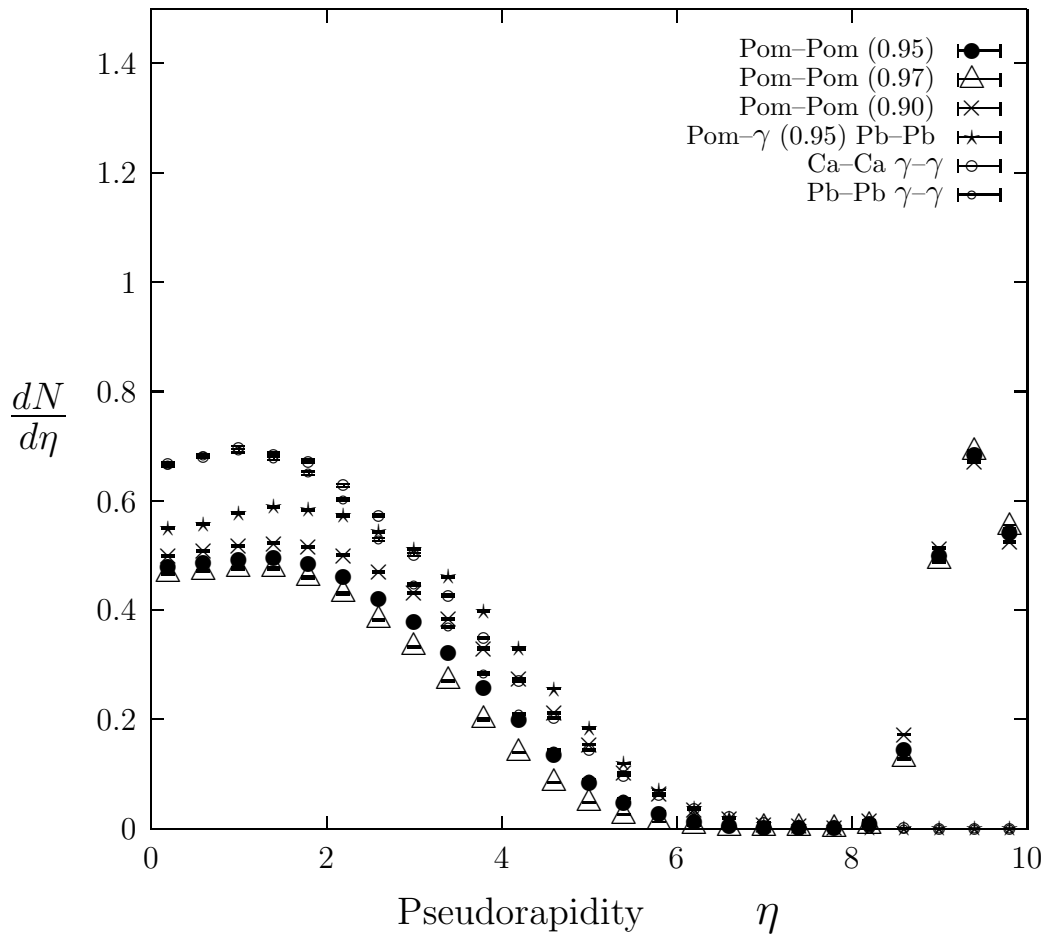


Figure 10: The pseudorapidity distribution of charged hadrons in photon-photon collisions in Pb-Pb and Ca-Ca heavy ion collisions (only the hadrons produced in the central cluster of particles are included in the histogram) compared to the corresponding distribution in central diffraction in pp collisions (in this case also the scattered original protons are included in the histogram) and to the corresponding distribution in photon-pomeron collisions in Pb-Pb collisions (in this case again only the hadrons in the central cluster are included in the histogram).

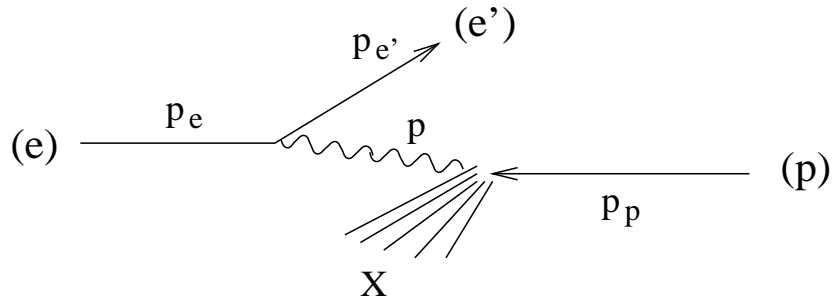


Figure 11: Diagram of ep scattering via one-photon exchange.

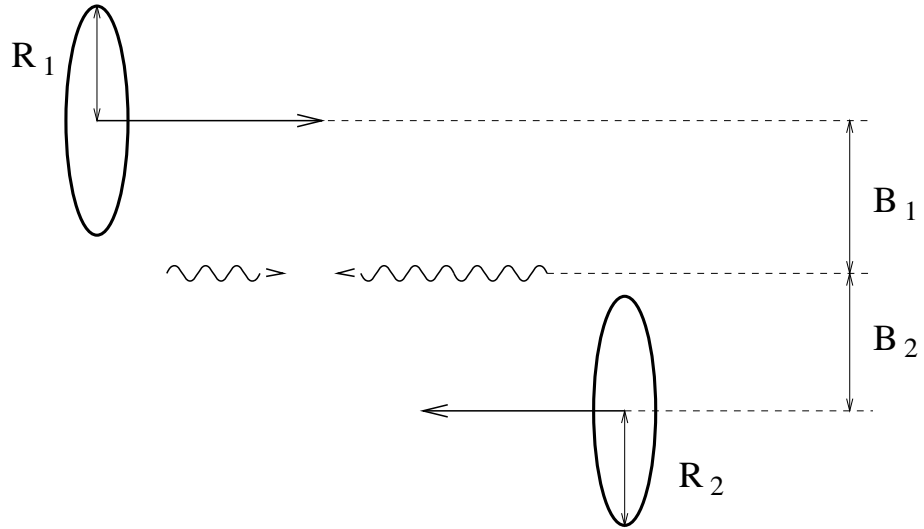


Figure 12: Semi-classical model of the photon-photon scattering in hadron-hadron interactions.

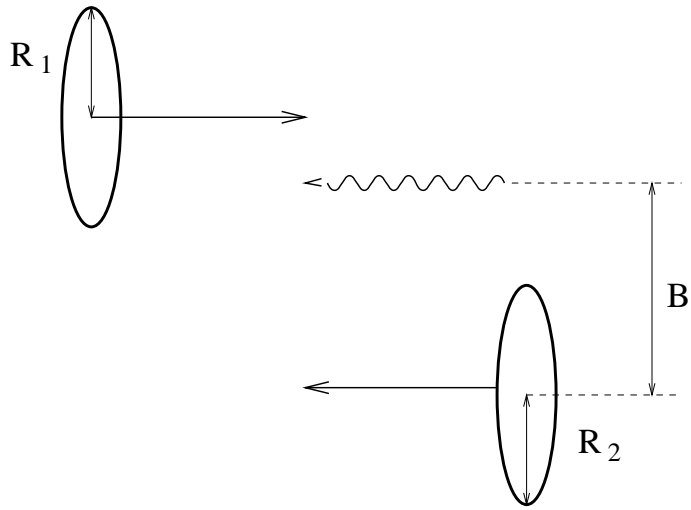


Figure 13: Semi-classical model of the photon-hadron scattering in hadron-hadron interactions. To obtain a model for photon-pomeron scattering, only single diffractive events where the photon dissociates are considered.